2025 IEEE Intelligent Vehicles Symposium (IV)
June 22-25, 2025. Cluj-Napoca, Romania

Lane-Keeping Guardian with Safety Filter: Experimental Validation

Illés Vörös, Xiao Li, Ilya Kolmanovsky, John Talbot,
James Dallas, Makoto Suminaka, John Subosits, and Gábor Orosz

***Abstract*— In this paper, a control barrier function (CBF) is constructed for the lane-keeping problem which is applicable to both human-driven and automated vehicles. Based on the resulting CBF, a safety filter is developed that prevents the vehicle from crossing the lane boundaries, while only modifying the nominal steering input when necessary. The effectiveness of the proposed control approach is demonstrated in a series of numerical simulations and real vehicle experiments with a human driver. The experimental results show that the safety filter can successfully keep the vehicle inside the lane boundaries by seamlessly modifying the steering input of the human driver in a minimally invasive manner.**

***Index Terms*— Lane-keeping control, safety filter, control barrier functions, advanced driver assistance systems**

2025 IEEE Intelligent Vehicles Symposium (IV) | 979-8-3315-3803-3/25/$31.00 ©2025 IEEE | DOI: 10.1109/IV64158.2025.11097430

I. Introduction

Recent advances in autonomous driving technologies have brought significant positive impacts in terms of technological and economic aspects [1], including improved driving comfort, enhanced fuel economy, and reduced traffic congestion. While such technologies have the potential to revolutionize transportation by reducing human error and improving mobility, ensuring the safety of these systems in a formally guaranteed manner is essential [2].

To provide provable safety assurance, researchers have extensively employed the model predictive control (MPC) framework as it directly handles constraints. MPC-based approaches in lateral vehicle control have been successfully implemented for lane-keeping [3], path tracking [4], [5] and regulating vehicle drifting trajectories [6], [7]. However, implementing MPC often involves solving nonlinear optimization problems onboard, which presents significant challenges in implementation [8]. Furthermore, integrating MPC with human control input is non-trivial, as the human control input is not known over the prediction horizon. Examples of shared control approaches based on nonlinear MPC include [9] and [10].

To reduce computational demands while preserving formal safety guarantees, approaches based on control barrier functions (CBFs) have been established [11]. With these methods, controllers are formulated as quadratic programs (QPs), where CBFs [12], incorporated as linear inequality constraints, enforce formal safety guarantees for the closed-loop system. These QPs are low dimensional and can even be solved explicitly in some cases, resulting in computationally efficient implementations. This framework also provides a natural way of integrating with human control inputs [13]. CBFs have been applied across a range of scenarios, including adaptive and connected cruise control [14], [15], emergency braking [16], and merge scenarios [17].

Several studies have investigated CBFs for lateral vehicle dynamics too: in [18] and [19], sum-of-squares optimization approaches were used to find suitable CBFs for lane-keeping. In [20], the lane-keeping and obstacle avoidance problem was approached based on Boolean compositions of multiple discrete-time CBFs, while [21] and [22] proposed using a combination of MPCs and CBFs.

However, the interaction of a CBF-based safety filter with a human driver has only been recently considered [23]. In this work, we analyze a safety filter for lane-keeping control with an emphasis on how it can provide formal safety guarantees in human-driven vehicles. As opposed to existing research, our proposed CBF includes a more precise consideration of the vehicle geometry when defining the safe set, including the yaw angle as well as the front and rear overhangs.

In non-safety critical situations, the driver maintains full control over the vehicle, without any modifications to their steering input (as opposed to several MPC-based approaches). Therefore, the feeling of driver control is not sacrificed inside the lane, while the seamless transitions between the steering input of the driver and the commanded steering signal of the safety filter can still prevent unintended lane departures. Note that the assessment of driver intent is assumed to be part of a higher-level decision logic. This falls outside the scope of the current study.

The results are demonstrated in a series of full-scale experiments on a test track, where a human driver intentionally tries to steer the vehicle out of the lane, while the safety filter successfully intervenes just enough such that safety is not compromised. This is achieved without any sudden jump in lateral acceleration and jerk.

The rest of the paper is organized as follows. Section II introduces the vehicle model used for control design. Section III presents a brief theoretical background on CBFs and the design process of the safety filter for lane-keeping. Numerical simulations are shown in Section IV to demonstrate the feasibility of the method. The experimental results are detailed in Section V, where the safety filter is implemented

Illés Vörös and Gábor Orosz are with the Department of Mechanical Engineering, University of Michigan, Ann Arbor, MI 48109, USA (email: illesvoe@umich.edu, orosz@umich.edu).

Xiao Li and Ilya Kolmanovsky are with the Department of Aerospace Engineering, University of Michigan, Ann Arbor, MI 48109, USA (email: hsiaoli@umich.edu, ilya@umich.edu).

John Talbot, James Dallas, Makoto Suminaka and John Subosits are with the Toyota Research Institute, Los Altos, CA 94022, USA (email: john.talbot@tri.global, james.dallas@tri.global, makoto.suminaka@tri.global, john.subosits@tri.global).

Gábor Orosz is also with the Department of Civil and Environmental Engineering, University of Michigan, Ann Arbor, MI 48109, USA.

on a human-driven vehicle, and Section VI concludes the results.

II. Vehicle Model

The safety filter design is based on an in-plane, kinematic bicycle model of the vehicle (see Fig. 1), where the side slip of the tires is neglected. The vehicle states include the position of the rear axle center point R (x_R and y_R) and the yaw angle ψ. The steering angle is denoted by δ and a constant longitudinal speed V is assumed. The corresponding equations of motion are

$$\dot{x}_\mathrm{R} = V\cos\psi, \quad \dot{y}_\mathrm{R} = V\sin\psi, \quad \dot{\psi} = \frac{V}{l}\tan\delta, \tag{1}$$

where l is the wheelbase.

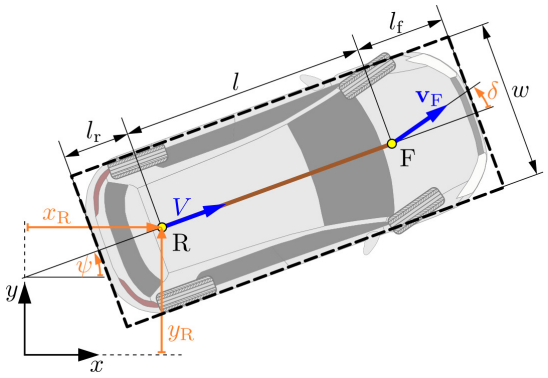

Fig. 1. Kinematic bicycle model used in this paper.

In order to account for the full length and width of the vehicle, a bounding box is defined according to the black dashed rectangle in Fig. 1. The width of the vehicle is denoted by w, and l_f and l_r are the front and rear overhangs, respectively.

III. Safety Filter Design

In this section, a safety filter is designed based on the vehicle model (1) in order to ensure that the vehicle stays inside the lane boundaries.

A. Control barrier functions

By considering $u = \tan\delta$ as the control input (and decoupling the longitudinal dynamics), the vehicle model (1) can be written in the control affine form

$$\dot{x} = f(x) + g(x)u, \tag{2}$$

with

$$x = \begin{bmatrix} y_\mathrm{R} \\ \psi \end{bmatrix}, \quad f(x) = \begin{bmatrix} V\sin\psi \\ 0 \end{bmatrix}, \quad g(x) = \begin{bmatrix} 0 \\ \frac{V}{l} \end{bmatrix}. \tag{3}$$

Note that $x \in \mathbb{R}\times(-\pi,\pi)$ and $u \in \mathbb{R} \Leftrightarrow \delta \in (-\frac{\pi}{2}, \frac{\pi}{2})$.

We maintain safety by rendering a safe set $\mathcal{S}$ in the state space $\mathbb{R}\times(-\pi,\pi)$ forward invariant, i.e., $\forall x(0) \in \mathcal{S} \Rightarrow x(t) \in \mathcal{S}, \forall t \geq 0$, see [12], [24]. To do so, a CBF $h : \mathbb{R}\times(-\pi,\pi) \to \mathbb{R}$ is constructed such that it is non-negative on $\mathcal{S}$:

$$\mathcal{S} = \{x \in \mathbb{R}\times(-\pi,\pi) : h(x) \geq 0\}. \tag{4}$$

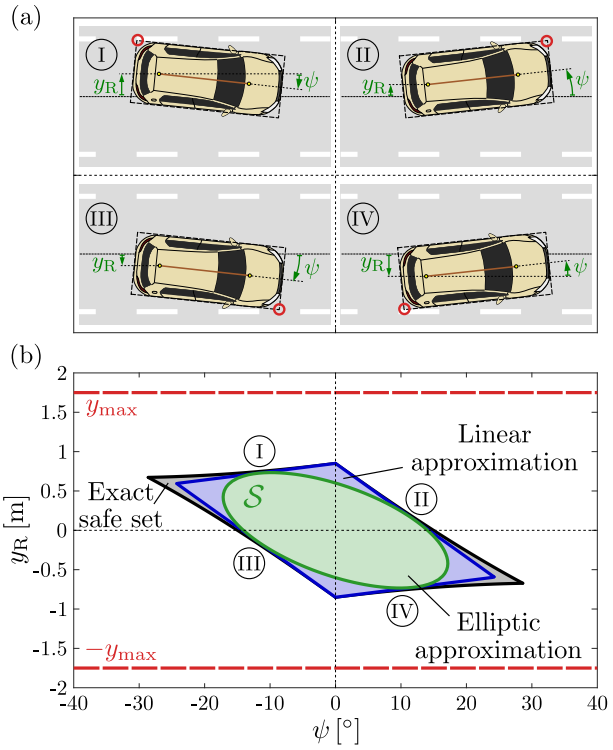

Fig. 2. (a) Vehicle configurations where one of the bounding box corners is touching the lane boundaries. (b) The exact safe set given by (9)–(12) (gray), its linear approximation (13)–(16) (blue), and the inscribed ellipse (17)–(18) (green).

Furthermore, the gradient of h must not disappear at the boundary of the safe set, i.e., $h(x) = 0 \Rightarrow \nabla h(x) \neq 0$. Once a CBF h is found, the forward invariance of $\mathcal{S}$ can be proven [12] if there exists a class-$\mathcal{K}$ function $\alpha : \mathbb{R}_{\geq 0} \to \mathbb{R}_{\geq 0}$ such that

$$\sup_{u\in\mathbb{R}} \underbrace{\left(\nabla h(x)f(x) + \nabla h(x)g(x)u\right)}_{\dot{h}(x,u)} > -\alpha\left(h(x)\right), \quad \forall x \in \mathcal{S}, \tag{5}$$

where in this paper the gradients are treated as row vectors.

To find a control law that deviates from the nominal control action $u_\mathrm{d}(x)$ (i.e., the steering input of the human driver) as little as possible, while still satisfying the safety condition (5), a quadratic program (QP) can be defined as follows:

$$u^*(x) = \underset{u\in\mathbb{R}}{\operatorname{argmin}} \|u - u_\mathrm{d}(x)\|^2, \quad \text{s.t.} \quad \dot{h}(x,u) \geq -\alpha\big(h(x)\big). \tag{6}$$

The closed-form solution to the optimization problem (6) in the single-input case is

$$u^*(x) = \begin{cases} \min\{u_\mathrm{d}(x), u_\mathrm{s}(x)\}, & \text{if} \quad \nabla h(x)g(x) < 0, \\ u_\mathrm{d}(x), & \text{if} \quad \nabla h(x)g(x) = 0, \\ \max\{u_\mathrm{d}(x), u_\mathrm{s}(x)\}, & \text{if} \quad \nabla h(x)g(x) > 0, \end{cases} \tag{7}$$

where

$$u_\mathrm{s}(x) = -\frac{\nabla h(x)f(x) + \alpha(h(x))}{\nabla h(x)g(x)}. \tag{8}$$

B. Safety filter for lane-keeping

In order to define the safe set $\mathcal{S}$ for the lane-keeping problem, we consider vehicle configurations where the entire bounding box is inside the lane boundaries (see Fig. 2(a)). The corresponding region in the plane of the yaw angle and the lateral position is bounded by four edges, each representing one of the corners of the bounding box touching a lane boundary. The front left and front right corners of the bounding box (cases II and III in Fig. 2(a)) stay inside the lane if

$$y_{\mathrm{R}} + (l + l_{\mathrm{f}}) \sin\psi + \frac{w}{2}\cos\psi < y_{\max}, \tag{9}$$

$$y_{\mathrm{R}} + (l + l_{\mathrm{f}}) \sin\psi - \frac{w}{2}\cos\psi > -y_{\max}, \tag{10}$$

respectively, where $+y_{\max}$ denotes the y coordinate of the left lane boundary, and $-y_{\max}$ is the y coordinate of the right lane boundary. Similarly, the conditions for the rear left and the rear right corners of the bounding box (cases I and IV in Fig. 2(a)) staying inside the lane are

$$y_{\mathrm{R}} - l_{\mathrm{r}} \sin\psi + \frac{w}{2}\cos\psi < y_{\max}, \tag{11}$$

$$y_{\mathrm{R}} - l_{\mathrm{r}} \sin\psi - \frac{w}{2}\cos\psi > -y_{\max}, \tag{12}$$

respectively.

The vehicle is considered safe if all four inequalities in (9)–(12) hold, i.e., the entire bounding box is inside the lane. The corresponding region of vehicle configurations is shown in gray in Fig. 2(b), where the roman numbers denote the edges representing the four cases in Fig. 2(a).

However, because of its non-smooth corners, the gray region cannot be directly used to construct a CBF. Therefore, we first linearize the inequalities in (9)–(12) around $\psi = 0$, leading to the blue parallelogram in Fig. 2(b) with sides

$$y_{\mathrm{R}} = \left(y_{\max} - \frac{w}{2}\right) - (l + l_{\mathrm{f}})\psi\,, \tag{13}$$

$$y_{\mathrm{R}} = -\left(y_{\max} - \frac{w}{2}\right) - (l + l_{\mathrm{f}})\psi\,, \tag{14}$$

$$y_{\mathrm{R}} = \left(y_{\max} - \frac{w}{2}\right) + l_{\mathrm{r}}\psi\,, \tag{15}$$

$$y_{\mathrm{R}} = -\left(y_{\max} - \frac{w}{2}\right) + l_{\mathrm{r}}\psi\,. \tag{16}$$

Then we derive the largest ellipse that can be inscribed inside the parallelogram (shown in green in Fig. 2(b)), which will be used as the safe set for the safety filter design. It can be shown that the largest ellipse inscribed inside a parallelogram touches the edges at the midpoints of the sides. The ellipse can be written in the form

$$F(\psi, y_{\mathrm{R}}) = a\psi^2 + b\psi y_{\mathrm{R}} + c y_{\mathrm{R}}^2 + d = 0, \tag{17}$$

where the parameters are

$$\begin{aligned} a &= -1, \quad b = -\frac{2(l + l_{\mathrm{f}} - l_{\mathrm{r}})}{(l + l_{\mathrm{f}})^2 + l_{\mathrm{r}}^2}, \\ c &= -\frac{2}{(l + l_{\mathrm{f}})^2 + l_{\mathrm{r}}^2}, \quad d = \frac{(2y_{\max} - w)^2}{4((l + l_{\mathrm{f}})^2 + l_{\mathrm{r}}^2)}. \end{aligned} \tag{18}$$

Using $h(x) = F(\psi, y_{\mathrm{R}})$ as CBF, the safe set is defined as

$$\mathcal{S} = \{y_{\mathrm{R}} \in \mathbb{R},\, \psi \in (-\pi, \pi) : F(\psi, y_{\mathrm{R}}) \geq 0\}. \tag{19}$$

The gradient of $h(x)$ can be calculated as

$$\nabla h(x) = \begin{bmatrix} b\psi + 2c y_{\mathrm{R}} & 2a\psi + b y_{\mathrm{R}} \end{bmatrix}, \tag{20}$$

which is only zero at the origin ($\psi = 0$, $y_{\mathrm{R}} = 0$).

Using (20) and (3), as well as the linear class-$\mathcal{K}$ function $\alpha(r) = \alpha_0 r$, (7) and (8) results in the safe lane-keeping controller with

$$u_{\mathrm{s}} = \frac{l\left(-V\sin\psi(b\psi + 2c y_{\mathrm{R}}) - \alpha_0(a\psi^2 + b y_{\mathrm{R}}\psi + c y_{\mathrm{R}}^2 + d)\right)}{V(2a\psi + b y_{\mathrm{R}})}. \tag{21}$$

IV. Numerical Simulations

In this section, numerical simulations are utilized to demonstrate how the safety filter can help the vehicle stay inside the lane boundaries. The parameter values are selected to match the test platform in Section V. In particular, $l = 2.8\,\mathrm{m}$, $l_{\mathrm{f}} = 0.6\,\mathrm{m}$, $l_{\mathrm{r}} = 0.6\,\mathrm{m}$ and $w = 1.8\,\mathrm{m}$. The half-width of the lane is $y_{\max} = 1.75\,\mathrm{m}$. In Fig. 3(a), the vehicle trajectory is plotted for $V = 8\,\mathrm{m/s}$ using the open-loop sinusoidal steering signal $\delta(t) = A\sin(\omega t)$, with $A = 5^\circ$ and $\omega = 1\,\mathrm{s}^{-1}$ (see the red line in Fig. 3(c)). The initial conditions ($y_{\mathrm{R}}(0) = 0\,\mathrm{m}$, $\psi(0) = -14.3^\circ$) were selected such that the vehicle oscillates symmetrically around the lane center line, repeatedly crossing the lane boundaries.

In Fig. 3(b), the same steering signal is used as the nominal controller u_{d}, but it is filtered through the safety filter introduced in Section III using $\alpha_0 = 1\,\mathrm{s}^{-1}$. This parameter can be used to fine-tune the responsiveness of the safety filter, i.e., how close it lets the system to the boundary of the safe set before intervening. In the orange trajectory segments, the sinusoidal steering is used without any changes, but as the vehicle approaches the boundary of the safe set, the safety filter switches to the safe input u_{s} (see the blue segments in Fig. 3(c)) to ensure that the vehicle does not leave the lane.

Figure 3(d) shows that despite the corrective actions of the safety filter, the lateral acceleration of the rear axle center point (apart from the initial correction at $\approx 4\,\mathrm{m/s^2}$) does not exceed $\approx 2\,\mathrm{m/s^2}$, ensuring a smooth ride. Note that the lateral acceleration of the rear axle can be calculated as $a_{\mathrm{R}}^{\mathrm{lat}} = -\ddot{x}_{\mathrm{R}}\sin\psi + \ddot{y}_{\mathrm{R}}\cos\psi$, which, using the time derivatives of (1), leads to $a_{\mathrm{R}}^{\mathrm{lat}} = \frac{V^2}{l}\tan\delta$.

The two vehicle trajectories are also plotted in the phase plane of the yaw angle and the lateral position in Fig. 3(e). It can be seen that without the safety filter (red trajectory), the vehicle barely stays inside the safe set (green ellipse), while the safety filter can indeed ensure that the boundary of the safe set is respected (see the orange/blue trajectory).

V. Experiments

In order to demonstrate the effectiveness of the proposed safety filter in aiding a human driver, a series of experiments were performed on a closed test track using the experimental platform in Fig. 4. During the experiments, the test vehicle was operated by a human driver whose steering inputs were filtered by the safety filter. In Section V-A, we present the details of the test vehicle, while the experimental results are included in Section V-B.

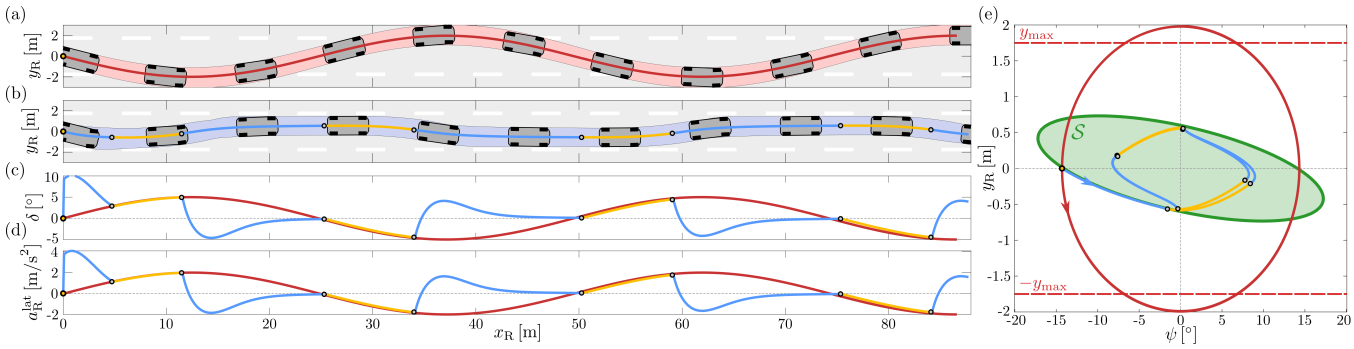

Fig. 3. Numerical simulations using sinusoidal steering: (a) vehicle trajectory without safety filter; (b) vehicle trajectory with safety filter; (c) steering angle signals: open-loop sinusoidal steering (red), nominal (orange) and safe (blue) inputs; (d) lateral acceleration of the rear axle center point; (e) phase portrait in the plane of yaw angle and lateral position.

Fig. 4. The test vehicle called GRIP.

A. Experimental platform

The test vehicle (called GRIP, see Fig. 4) is a custom-built drive-by-wire platform with four independent in-hub motors and front and rear-wheel steering (the rear-wheel steering of the vehicle was not used in the experiments). The vehicle is equipped with a dual antenna RTK-GPS/IMU system that provides state information at 200 Hz. The safety filter was implemented on an onboard computer and was executed at the same 200 Hz rate.

B. Experimental results

The experiments were performed on a closed skidpad at a constant speed, which was ensured by a proportional longitudinal controller. Each test run started with an acceleration phase where the longitudinal controller accelerated the vehicle to the desired speed. The longitudinal controller stayed active for the remainder of the experiment to keep the vehicle speed steady. Once the desired speed was reached, a virtual lane (of half-width $y_{\max} = 1.75\,\mathrm{m}$) was generated around the current position and orientation of the vehicle, which ensured the accuracy and repeatability of the initial conditions. Note that the human driver did not actually see the lane boundaries during the experiments, he was only aware that the vehicle was approximately in the center of the lane at the start. Furthermore, he could get a sense of the lane boundaries based on the response from the safety filter as he was trying to steer the vehicle out of the lane.

Three different longitudinal speeds were used in the experiments ($V = 6\,\mathrm{m/s}$, $8\,\mathrm{m/s}$ and $10\,\mathrm{m/s}$, see Figs. 5, 6 and 7, respectively) and the class-$\mathcal{K}$ function parameter α_0 was set to $1\,\mathrm{s}^{-1}$ in the safety filter. Panels (a) of Fig. 5–7 show aerial footage of the vehicle during the measurements, with the trajectory of the rear axle center point overlaid from the GPS data. The orange circles at $x_R = 0\,\mathrm{m}$ denote the end of the acceleration phase, at which point the lane boundaries (red dashed lines) were generated according to the initial conditions $\psi = 0°$, $y_R = 0.1\,\mathrm{m}$. In the orange trajectory segments, the commanded steering angle of the human driver is realized, while in the blue segments, the safety filter overrides the commanded input to ensure that the vehicle stays inside the lane.

Panels (b) of Fig. 5–7 show both the commanded (red dashed lines) and the realized (orange/blue) steering angles along the vehicle trajectories. It can be seen that as the vehicle starts moving closer to the lane boundaries, the safety filter intervenes and steers the vehicle back towards the center of the lane with a yaw angle of $\psi \approx 0$. Some delay can be observed between changes in the steering angle and the yawing of the vehicle, which suggests the presence of some compliance in the steering system and tire dynamics. Note that the safety filter only prevents crossing the lane boundaries, it does not aim to follow the lane center line exactly. Once the vehicle is sufficiently safe, it hands back full control to the driver.

The lateral acceleration of the rear axle center point R is plotted in panels (c) of Figs. 5–7. Even though the safety filter changes the steering angle abruptly in safety-critical situations, the lateral acceleration still remains below $2\,\mathrm{m/s}^2$. Furthermore, since the safety filter aims to minimize the difference between the driver's input and the safe input, control is handed back to the human driver in a smooth manner, without sudden jumps in the lateral acceleration.

The measured vehicle trajectories in the phase plane of the yaw angle and the lateral position are plotted in Fig. 8. Even though the trajectories slightly exit the safe set $\mathcal{S}$ at certain places, the vehicle still stays inside the lane boundaries. This is because the ellipse used as CBF is a conservative approximation of the exact safe set (see Fig. 2), therefore some violation of the safety constraint due to modeling errors is compensated.

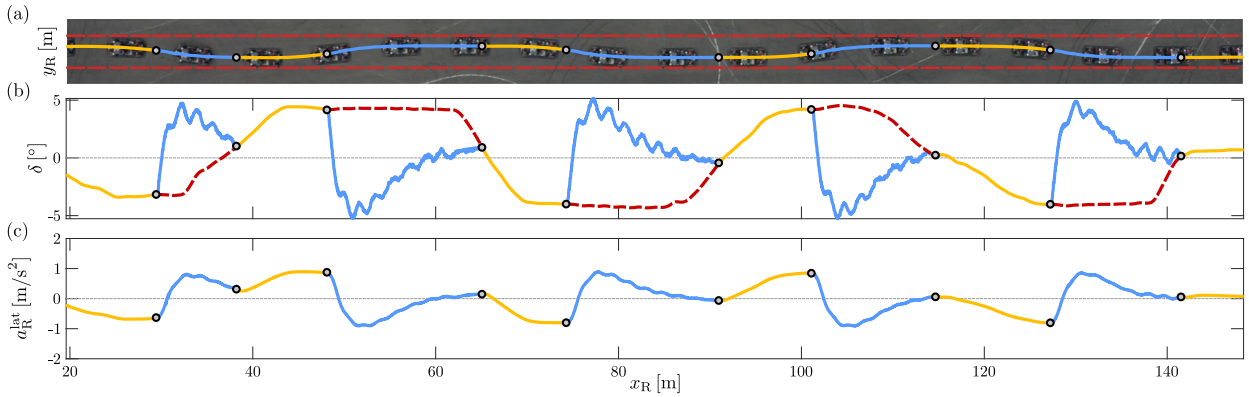

Fig. 5. Experimental results for $V = 6$ m/s: (a) aerial view of the measurement with the trajectory of the rear axle center point, (b) commanded steering input by the human driver (red dashed lines) and the measured steering angle at the wheels (orange/blue lines), (c) lateral acceleration of point R.

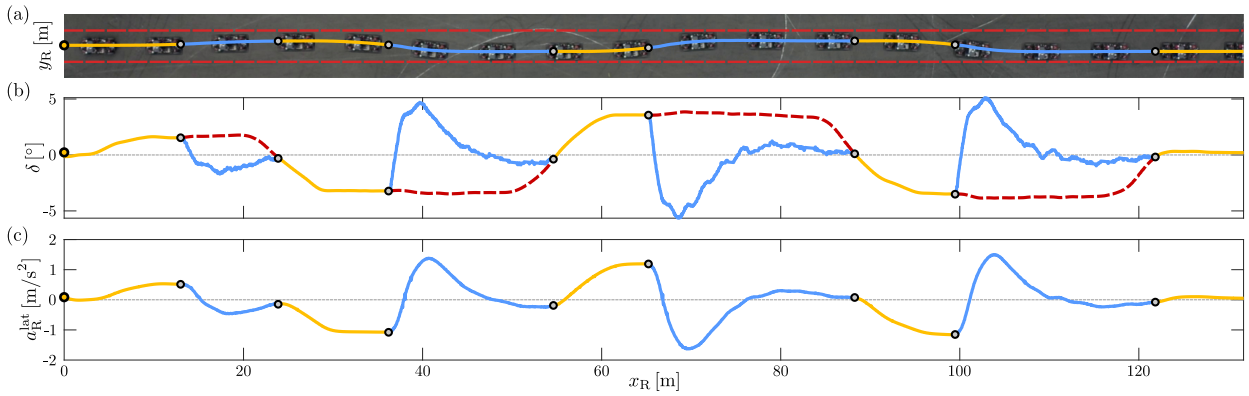

Fig. 6. Experimental results for $V = 8$ m/s: (a) aerial view of the measurement with the trajectory of the rear axle center point, (b) commanded steering input by the human driver (red dashed lines) and the measured steering angle at the wheels (orange/blue lines), (c) lateral acceleration of point R.

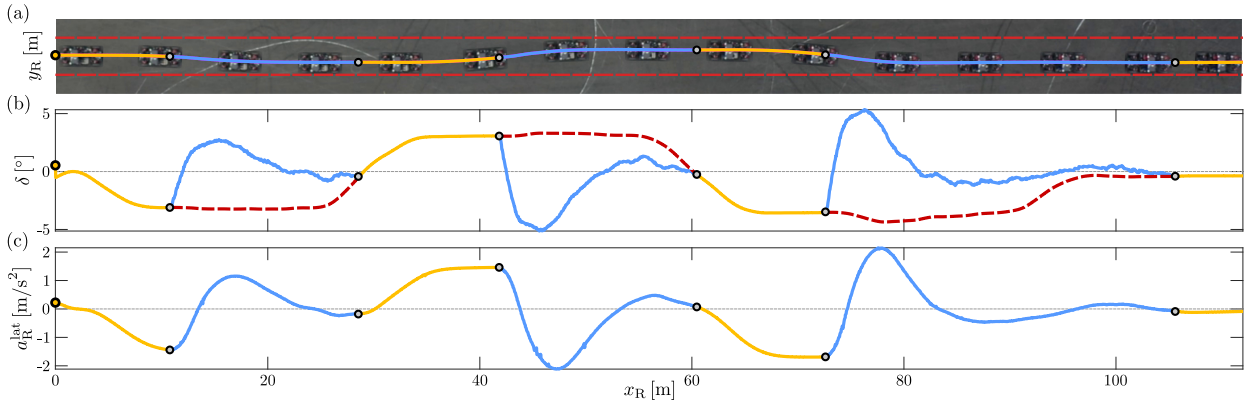

Fig. 7. Experimental results for $V = 10$ m/s: (a) aerial view of the measurement with the trajectory of the rear axle center point, (b) commanded steering input by the human driver (red dashed lines) and the measured steering angle at the wheels (orange/blue lines), (c) lateral acceleration of point R.

VI. Conclusion

A safety filter for lane-keeping control was presented in this paper. The safe set for the lane-keeping problem was defined in the plane of the lateral position and yaw angle of the vehicle based on geometrical considerations, and a corresponding smooth control barrier function was constructed. Based on the resulting CBF and a kinematic vehicle model, a safety filter was designed and tested in a series of numerical simulations and real vehicle experiments. Thanks to the closed-form solution of the corresponding optimization problem, the computational requirements of the resulting controller are negligible. The experimental results demonstrated that the safety filter is able to successfully aid the human driver in preventing unintended lane departures while maintaining a comfortable ride.

In order to successfully apply the safety filter at higher speed levels too, the vehicle model should be extended with the consideration of tire dynamics and the compliance of the steering system. Additional future research directions include a more thorough analysis of the effects of the class-

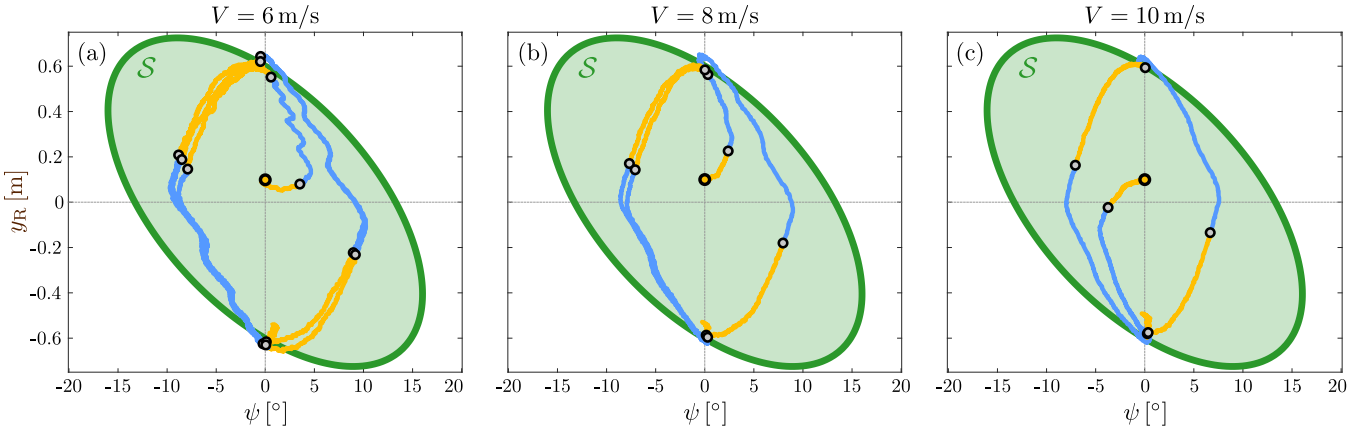

Fig. 8. Measured vehicle trajectories in the plane of yaw angle and lateral position. Orange: steering command by human driver is realized, blue: safety filter is active.

$\mathcal{K}$ function selection, the consideration of variable vehicle speed, and more in-depth analysis of how the safety filter affects the feeling of driver control.

Acknowledgment

This research was supported by the Toyota Research Institute (TRI). G. Orosz acknowledges the support of the Hungarian Academy of Sciences within the Distinguished Guest Fellowship Programme and the support of the Fulbright Foundation. I. Vörös was supported by the Rosztoczy Foundation.

References

[1] M. Maurer, J. C. Gerdes, B. Lenz, and H. Winner, *Autonomous driving: technical, legal and social aspects*. Springer Nature, 2016.

[2] S. Shalev-Shwartz, S. Shammah, and A. Shashua, "On a formal model of safe and scalable self-driving cars," *arXiv preprint arXiv:1708.06374*, 2017.

[3] M. Bujarbaruah, X. Zhang, H. E. Tseng, and F. Borrelli, "Adaptive MPC for autonomous lane keeping," in *14th International Symposium on Advanced Vehicle Control (AVEC)*, 2018.

[4] V. Turri, A. Carvalho, H. E. Tseng, K. H. Johansson, and F. Borrelli, "Linear model predictive control for lane keeping and obstacle avoidance on low curvature roads," in *16th IEEE International Conference on Intelligent Transportation Systems (ITSC)*. IEEE, 2013, pp. 378–383.

[5] F. Borrelli, P. Falcone, T. Keviczky, J. Asgari, and D. Hrovat, "Mpc-based approach to active steering for autonomous vehicle systems," *International Journal of Vehicle Autonomous Systems*, vol. 3, no. 2-4, pp. 265–291, 2005.

[6] T. P. Weber and J. C. Gerdes, "Modeling and control for dynamic drifting trajectories," *IEEE Transactions on Intelligent Vehicles*, vol. 9, no. 2, pp. 3731–3741, 2024.

[7] J. Y. M. Goh, M. Thompson, J. Dallas, and A. Balachandran, "Beyond the stable handling limits: nonlinear model predictive control for highly transient autonomous drifting," *Vehicle System Dynamics*, vol. 62, no. 10, p. 2590–2613, 2024.

[8] M. Diehl, H. J. Ferreau, and N. Haverbeke, "Efficient numerical methods for nonlinear MPC and moving horizon estimation," in *Nonlinear Model Predictive Control: Towards New Challenging Applications*. Springer, 2009, pp. 391–417.

[9] I. Karino, J. Dallas, and Y. M. Jonathan Goh, "Shared control for giving ordinary drivers expert level drifting skills," in *IEEE International Conference on Systems, Man, and Cybernetics (SMC)*, 2023, pp. 1461–1467.

[10] J. Dallas, I. Karino, M. Thompson, B. Araki, S. Goldine, Y. M. J. Goh, and J. Subosits, "Safe stability envelopes and shared control for active vehicle safety," in *IEEE Conference on Control Technology and Applications (CCTA)*, 2024, pp. 561–568.

[11] A. D. Ames, X. Xu, J. W. Grizzle, and P. Tabuada, "Control barrier function based quadratic programs for safety critical systems," *IEEE Transactions on Automatic Control*, vol. 62, no. 8, pp. 3861–3876, 2017.

[12] A. D. Ames, S. Coogan, M. Egerstedt, G. Notomista, K. Sreenath, and P. Tabuada, "Control barrier functions: Theory and applications," in *European Control Conference (ECC)*. IEEE, 2019, pp. 3420–3431.

[13] T. G. Molnar, S. K. Kannan, J. Cunningham, K. Dunlap, K. L. Hobbs, and A. D. Ames, "Collision avoidance and geofencing for fixed-wing aircraft with control barrier functions," *arXiv preprint arXiv:2403.02508*, 2024.

[14] A. D. Ames, J. W. Grizzle, and P. Tabuada, "Control barrier function based quadratic programs with application to adaptive cruise control," in *53rd IEEE Conference on Decision and Control (CDC)*. IEEE, 2014, pp. 6271–6278.

[15] Y. Chen, G. Orosz, and T. G. Molnar, "Safe and stable connected cruise control for connected automated vehicles with response lag," *arXiv preprint arXiv:2409.06884*, 2024.

[16] A. Alan, A. J. Taylor, C. R. He, A. D. Ames, and G. Orosz, "Control barrier functions and input-to-state safety with application to automated vehicles," *IEEE Transactions on Control Systems Technology*, vol. 31, no. 6, pp. 2744–2759, 2023.

[17] V.-A. Le, H. M. Wang, G. Orosz, and A. A. Malikopoulos, "Coordination for connected automated vehicles at merging roadways in mixed traffic environment," in *62nd IEEE Conference on Decision and Control (CDC)*. IEEE, 2023, pp. 4150–4155.

[18] X. Xu, J. W. Grizzle, P. Tabuada, and A. D. Ames, "Correctness guarantees for the composition of lane keeping and adaptive cruise control," *IEEE Transactions on Automation Science and Engineering*, vol. 15, no. 3, pp. 1216–1229, 2017.

[19] Y. Duan and X. Zeng, "Computational synthesis of control barrier functions with applications in automotive lane keeping supervisory control," *IET Control Theory & Applications*, vol. 17, no. 14, pp. 1894–1908, 2023.

[20] M. Cavorsi, M. Khajenejad, R. Niu, Q. Shen, and S. Z. Yong, "Tractable compositions of discrete-time control barrier functions with application to lane keeping and obstacle avoidance," in *Europecan Control Conference (ECC)*, 2021, pp. 1303–1309.

[21] S. Brüggemann, D. Steeves, and M. Krstic, "Simultaneous lane-keeping and obstacle avoidance by combining model predictive control and control barrier functions," in *61st IEEE Conference on Decision and Control (CDC)*. IEEE, 2022, pp. 5285–5290.

[22] T. D. Son and Q. Nguyen, "Safety-critical control for non-affine nonlinear systems with application on autonomous vehicle," in *58th IEEE Conference on Decision and Control (CDC)*. IEEE, 2019, pp. 7623–7628.

[23] J. Dallas, J. Talbot, M. Suminaka, M. Thompson, T. Lew, G. Orosz, and J. Subosits, "Control barrier functions for shared control and vehicle safety," *arXiv preprint arXiv:2503.19994*, 2025.

[24] T. G. Molnár, G. Orosz, and A. D. Ames, "On the safety of connected cruise control: analysis and synthesis with control barrier functions," in *62nd IEEE Conference on Decision and Control (CDC)*. IEEE, 2023, pp. 1106–1111.